Chapter 10
Density Functional Theory (DFT) Study of Novel 2D and 3D Materials

Fayyaz Hussain, Muhammad Imran and Hafeez Ullah

10.1 Introduction

In modern era, conventional semiconductors exhibiting ferromagnetism called diluted magnetic semiconductors (DMSs) are acquired after doping various kinds of transition metals (TMs). In the last 20 years, at the room temperature, DMSs have exhibited auspicious ferromagnetism. As a result, an incredible interest has been bred for the forthcoming spintronics applications [1–3]. It opens new inroads of DMSs for the future spintronics materials having distinguished features and potential applications comprising of fast memory speed, ultra-grade lowers the power consumption, logic photonic devices, and bio-detectors [4–7]. The ferromagnetism at room temperature could be obtained by the magnetic doping of materials (semiconductors) having wide band gap [1]; usually, ferromagnetism at room temperature has been found in TiO_2, GaN, ZnO doped with Cr, Co, Fe, and Mn [8–10]. For doping elements, local magnetic moments are not the finest way, so in DMSs, local magnetic cluster has been exposed for being ferromagnetic (FM) that is not worthy for the FM [11–14]. The Cu being a hot dopant has

F. Hussain (✉)
Material Simulation Research Laboratory (MSRL), Department of Physics,
Bahauddin Zakariya University, Multan 60800, Pakistan
e-mail: fayyazhussain248@yahoo.com

H. Ullah (✉)
Department of Physics, The Islamia University of Bahawalpur,
Bahawalpur 63100, Pakistan
e-mail: hafeezullah79@gmail.com

M. Imran
Department of Physics, Govt. College University Faisalabad,
Faisalabad 38000, Pakistan
e-mail: imraniub86@gmail.com

© Springer Nature Singapore Pte Ltd. 2017

Z.H. Khan (ed.), *Recent Trends in Nanomaterials*,
Advanced Structured Materials 83, DOI 10.1007/978-981-10-3842-6_10

acquired theoretical as well as experimental attention. Currently several experimental attempts have been reported to predict the ferromagnetism in Cu doped ZnO at room temperature [15–19].

Metal and the metal oxide (M/O) system is extensively used in all kinds of catalysis and microelectronics functions such as Schottky barrier diode, laser diode, and ultraviolet (UV) diode [20, 21]. Most recent attempts to decrease the dimension of electronic devices (as small as one atom thick) have been done using boron nitride and graphene like nanomaterials [22–25]. For this reason, lots of studies have been done on monolayer based BN nanostructure and graphene, for example, nanoflakes, nanoribbons, and their hybrid structures [26–30]. Most recent attempt has been prolonged toward other materials of two dimensions (2D). ZnO is known to be very favorable for the fabrication of UV light emitter and microelectronics, for catalysis, and for gas sensing [31, 32]. The crystal that has polar surfaces, such as low-index surface of ZnO [33], it displays stronger surface reconstruction and is generally enough stable [34]. Currently, Tseng et al. adop sol-gel technique to synthesis ZnO nanostructure in 1D, 2D, and 3D spherical crystals [35]. Therefore, nanosheet of ZnO is a powerful applicant for catalysis and microelectronic functions.

Diamond (film) acts as a fantastic practical material because of its precious characteristics such as extraordinary carrier mobility (for holes: 1600 $cm^2\ V^{-1}\ s^{-1}$ and for electrons: 2200 $cm^2\ V^{-1}\ s^{-1}$), sharp energy gap ($\sim$5.5 eV), good thermal conductivity (2600 $W\ m^{-1}\ K^{-1}$) hence has prospective commercial applications, such as photodiode, radiation detectors, and heterojunction [36]. In addition, in diamond, the doping of outsized atomic elements is not appropriate since they produce greater lattice distortion while doping of smaller sized elements plays very important role in order to boost its value for electrochemical and electronics devices [37–39]. It is too easy to achieve thin films of p-type diamond by doping boron in diamond [40–42]. However, it is much harder to fabricate thin films of n-type diamond by doping As, P, N, S, Na, Li, etc. [43–48] because in diamond structure between C–C, there is smaller lattice space. It is assumed that the incorporation of bcc tantalum film into diamond will be helpful to decrease resistivity without declining mechanical properties, since Ta is chemically active, ductile, and soft and its resistivity is smaller (15–70 μΩ cm) [49].

Latest advanced studies suggest that the magnetization in carbon (diamond) is because of the defects in it [50–54] which tend to make this material a powerful candidate for future spintronics applications [55, 56]. In addition, the thin films of p-type can be simply obtained after boron doping [42, 57]. While it is more challenging to acquire n-type diamond [43, 44], further its progress is very important for electronic progress applications and many more materials [58]. The indium dopant is considered to be the finest donor in order to develop an n-type diamond. However, it has been a challenging feature for computational field to develop a theoretical model of oxygen-doped diamond due to its chemical nature.

10.2 The Method of Calculations

All calculations are carried out within plane-wave density functional theory (DFT) by employing the Vienna ab initio simulation package (VASP) [59, 60]. The generalized gradient approximation (GGA) with the Perdew, Burke, and Ernzerhof (PBE) of function and projector augmented wave (PAW) potential are selected in all these DFT calculations [61–63]. The vacuum surface is set to be 14 Å for the 2D system along c-direction, and it is not required for 3D materials calculations. The convergence tests for both systems of total energy with respect to the electron wave function are expanded using plane waves with a cutoff energy of 400 eV. The ionic position, cell volume, and lattice parameters of the system are fully relaxed with conjugate gradient method until the Hellmann Feynman forces are smaller than 0.02 eV/Å and the energy convergence criteria are met 1×10^{-5} eV. Hybrid Functional corrections (HSE 06) [64] have been applied to get more accurate band gap. The popular scheme for this calculation is Monkhorst-pack (MP) [65, 66] which is applied for K-point sampling.

10.3 Results and Discussion

10.3.1 Diluted Magnetic Semiconductors (DMSs)

The (0001) surface of GaN is renowned not only from the theoretical perspective but from the experimental too [67–74]. Currently to find out a fairly stable structure, numerous positions of adatom have been examined. On (0001) surface of GaN, T1, T4, and H3 positions are highly symmetric points, as reported T4 be the more auspicious site for adsorption [75]. We remove one Ga atom and substitute a Cu atom. After the substitution, the lattice parameter (−0.006 Å) changes slightly. Basically, this happens because of the different atomic radius of Ga from Cu and all the bond lengths of Cu-N3 system are of 2.0 Å. In GaN (2D layer), the magnetization per Cu atom is 2.0 μB and is in harmony to Wu et al. [76], but its value is larger than the value of ZnO doped with Cu [77]. Figure 10.1 shows the spin charge density of N-2p and Cu-3d.

The FM coupling is noticed to be the stronger coupling in N-2p atoms because these are close to Cu-3d showing that the Cu-3d atom being responsible for FM coupling in the system. Figure 10.2 shows the resolved spin band structure of GaN 2D layer.

The majority spin channel (blue) is for semiconductor while the minority spin channel (red) exhibits metallic characteristic with sufficient unfilled states on the right side of Fermi level as reported in also Ref. [76].

The unfilled states are extremely valuable for conduction charge carriers (compulsory for adequate spin polarized current) [79, 80]; hence, its 2D Cu-doped GaN layer is suggested to be used as injection of spin charge carriers. In the previous study of magnetic coupling, similar method was adopted [76].

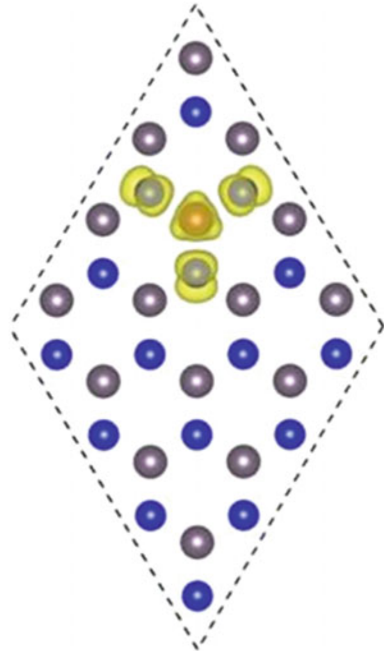

Fig. 10.1 Isosurface of spin charge density of 2D GaN layer doped with 6.25% of Cu [78]

We substitute, for antiferromagnetic (AFM) and FM coupling, two Cu atoms along c-direction separated 5.82 Å distant apart. For both systems, the total energy is calculated and the results indicate FM state to be the ground state having energy of 173 meV, that is, lower energy than AFM state. In DOS, p and d orbitals are represented by the red and blue curves, respectively, shown in Fig. 10.3 exhibiting semiconducting character. In 2D GaN DMSs doped with Cu to understand the responsible mechanism for the stabilization of FM state in Fig. 10.4, the projected density of states (PDOSs) plot for Cu and its nearest neighboring N atoms are shown.

The majority spin channel shows the coupling between N-2p and Cu-3d is strong; in case of Cu-3d, an interaction peak is noticed at −0.43 eV which overlaps with N-2p in Cu-N3, while for Cu-3d, the second interaction peak is noticed at −0.37 eV which overlaps with N-2p through smaller magnetization. In case of minority spin channel, the significant contribution toward the unoccupied states is because of 2p state of three connecting N atoms. These features specify that the coupling of Cu atom with its three neighbor atoms of N is a strong coupling. Due to the strong hybridization, a finite magnetization has been persuaded on Cu and its neighboring N atoms. The magnetization of 0.25 μB is carried by each N atom, and in case of Cu atom, the magnetization is of the magnitude of 0.56 μB. This value of magnetization is similar for N as deliberated in Ref. [76] while the value of magnetization of 0.14 μB in case of Cu is smaller in GaN 2D layer than GaN bulk, however, greater as compared to Mn in the Mn-doped GaN [81]. The magnetization

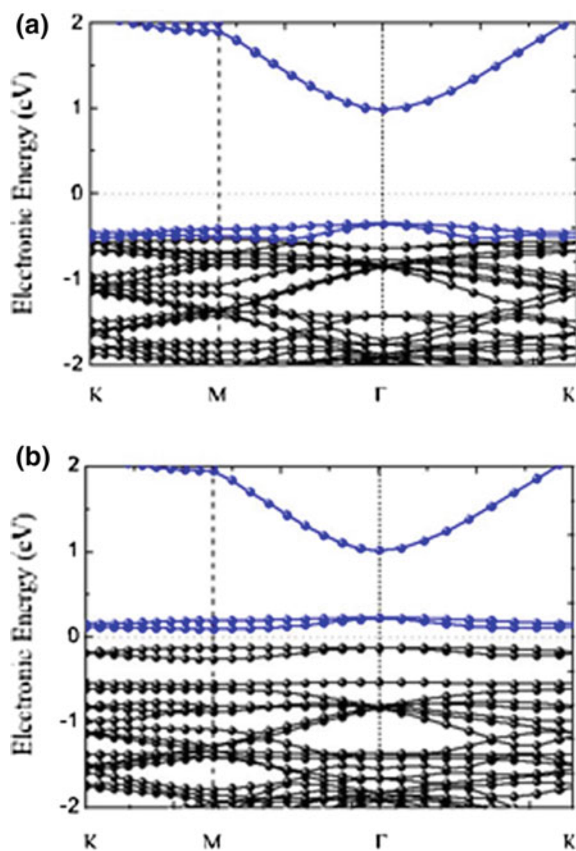

Fig. 10.2 Band structure of **a** majority spin **b** minority spin of 2D GaN layer doped with 6.25% of Cu [78]

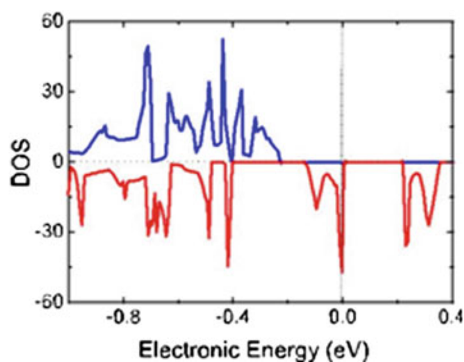

Fig. 10.3 Spin polarized DOSs of Cu-3d and N-2p [78]

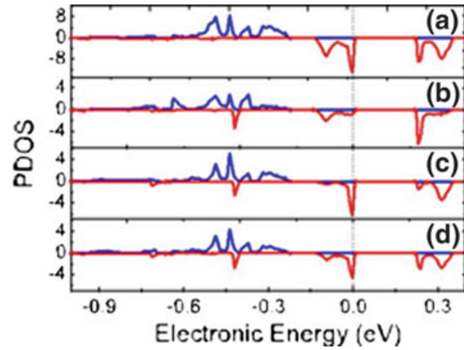

Fig. 10.4 Spin PDOSs of Cu-3d (**a**) and N-2p of the N atoms in CuN_3 structure (**b–d**) [78]

of every single N atom linked to Mn is smaller than 0.02 μB instead of greater magnetization of 4 μB of Mn; hence, in case of Cu-doped 2D GaN for ferromagnetism, the hybridization of p-d orbitals is responsible.

10.3.2 Semiconductor and Metal Interface

For a metal/semiconductor contact, the charge carriers on the two sides of the interface redistribute and reach an equilibrium state upon adjusting the Fermi levels of the two phases. The schematic diagram of the energy band structures of ZnO and Cu metal before and after contact is shown in Fig. 10.5.

However, in present study, we just consider ZnO layer to be atomically thin, and the band arrangement for multilayer sheets of ZnO with Cu assumed to be like single sheet because of layers' weak interaction [82]. So as to study the relative energy level shifting of Cu and ZnO, a reference vacuum level of (2D) Cu, ZnO, and Cu-ZnO hybrid system is aligned. Physically, for the alignment of Fermi level across interface, the electrons are transferred from the substrate (Cu) toward the semiconducting layer (ZnO); as a result, the electrons accumulate at interface in the form of extremely thin region. Hence, after the achievement of the state of equilibrium of electronic charge, further flow from metal layer toward the semiconductor layer slows down. Figure 10.6a shows the addition in carrier charge density at interface than ZnO layer, due to the deposition of ZnO monolayer under equilibrium, upon metal substrate. In order to calculate the work function, Fermi level is subtracted from electrostatic potential [83]. In Fig. 10.6, we have lined up a (uniform) reference vacuum level to study the relative energy level shift of 2D ZnO layer.

The value of work function for polar (0001) ZnO is estimated to be 4.68 eV. In case of ZnO films, the value of work function calculated using Schottky barrier model lies in the range from 4.45 to 4.50 eV [84]. The value of effective work

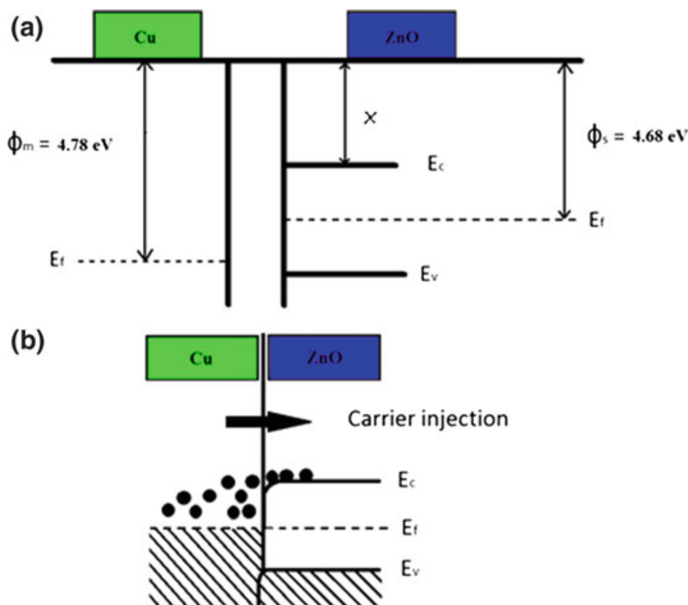

Fig. 10.5 Schematic diagrams of the energy band structures of ZnO and Cu metal. **a** Before contact and **b** after contact

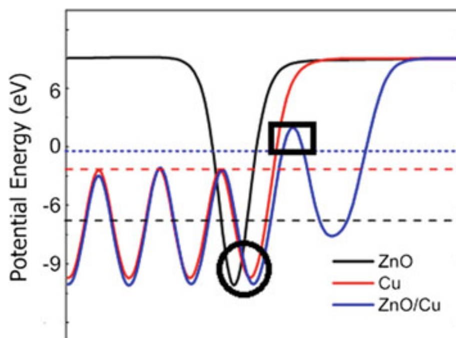

Fig. 10.6 Work function plot, potential lineups of ZnO, Cu, and ZnO–Cu hybrid. The *black rectangular box* indicates the tunneling barrier and *circle* shows shifting of energy states

function for n-type ZnO has been reported to be 4.45 eV, and the value of 4.29 eV has been reported for electron affinity of ZnO [85]. Furthermore, it is found that in ZnO the presence of oxygen defect causes its work function to be reduced. The value of work function in case of Cu substrate calculated is 4.78 eV. This value of work function is in close agreement with that of experimentally estimated value of 4.54 eV for Cu [86]. In the consequence, the development of Schottky contact at the interface of Cu and ZnO 2D monolayer is expected, along with the accumulation of electrons (majority carriers) in between the interfacial layer and within the layer of ZnO. A large number of carriers inject into semiconductor (ZnO) layer,

when the difference of work function is greater. It is the leading reason of which conductivity of multilayer structure has been increased. The injection of majority carrier electrons occurs from Cu substrate toward ZnO layer. These electrons attract the positively charged ions after their accumulation in conduction band. Figure 10.6 exhibits the transfer of charge from Cu substrate to ZnO monolayer. Recently, the established electric field has its direction from positively charged atoms (Cu) toward the conduction band electrons. An observed tunneling barrier at interface is shown by a black rectangular box in Fig. 10.6. Tunneling probability has been estimated at ZnO–Cu interface system, supposing a square potential barrier of width 1.12 Å and height 0.97 eV. This behavior has a good accordance with recent study of Ag-G system presented by Gong et al. [87] also with experimental results of Vogel et al. [88]. The contact can be a Schottky or an ohmic. The type of interface between semiconductor and the metal and the alignment of Fermi surface determines the sort of contact. This also relies on the kind of majority carriers (holes or electrons) and also on the work function (φ) of semiconducting materials and the metal. In the case of n-type semiconductor, a Schottky barrier is formed when the work function of metal (φ_M) used for contact is greater than the work function of semiconductor (φ_S). In our current work, the work function of Cu (φ_M) is greater than that of ZnO (φ_S), so the contact is Schottky contact. According to the Davidos, Mott, and Schottky theories [89], the height of barrier (φ_B) can be found using following equation:

$$\varphi_B = \varphi_M - \chi_S$$

The symbol χ_S represents the electron affinity of semiconducting material.

The existence of oxide layer because of pinning must cause a large value of φ_B (shift of the height of barrier) through some charge transfer. For essential shift of levels to be occurred, the massive charge transfer and the definite value of shifted charge could be relatively small. Because of this transfer of charge, an attractive force due to ionization develops at interface and causes change in the Fermi level making it act as a slightly forward bias efficiently; therefore, the height of Schottky barrier and band bending will be lessened. In 1947, Bardeen explained this Schottky barrier height in his theory [90].

For both systems, Fig. 10.7 displays the PDOS in which the ZnO valence band is mostly comprised of p-orbital of oxygen and d-orbital of Zn. In case of Cu, the conduction as well as valence bands are mainly comprised of d-orbital.

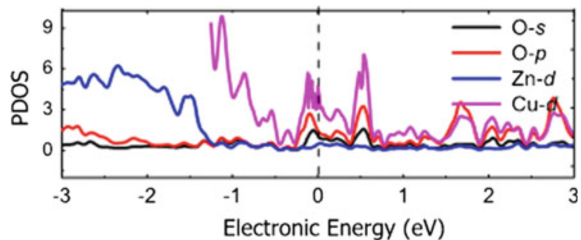

Fig. 10.7 PDOS after contact of hybrid system ZnO/Cu

In the case of hybrid system, the contribution of s and p atomic orbitals of O atom in the conduction band is small while the 3d Cu atom orbital is larger. For both ZnO and Cu phases, there exist sharp peaks in the region of low energy of conduction as well as valance band. For Cu, these peaks are more obvious. The hybridization of d-d orbitals is responsible for sharpness of peaks, and these peaks can be separated into two groups below and above the Fermi level, respectively. In comparison with pure Cu, the 3d-Cu states in the case of hybrid system of valance band states shift forward to higher energy near Fermi level. Figure 10.7 clarifies that in case of pristine ZnO layer, only contribution for valance band is from hybridization of s-p orbital of O atom. Anyhow, in case of hybrid system, the p states of O atom have major component in the conduction band also around Fermi level that is chiefly due to the hybridization of O-p and 3d-4s states of Cu. Additionally, the shifting of Zn-3d states toward valance band makes a sharp peak of value −2.35 eV.

10.3.3 Effects of Tantalum Incorporation into Diamond Films

In order to understand the electronic properties of the Ta-incorporated diamond films, their band structures (BSs) have been elaborated by using first principle calculations which are reported in [91]. The diamond films BSs substitutionally doped with Ta impurity, and pure diamond film's BSs energy gap is ~4.4 eV [92]. Band structures of 1.56% Ta-doped diamond films, for minority (↓) and majority (↑) electronic spins reported in [91]. The formation of impurity states occur within the region of band gaps near conduction band minimum (CBM). From band structure plot of Ta-incorporated diamond, the distribution of a large number of (n-type) impurity states between Fermi level and conduction band can be observed. Spin-up and spin-down electrons may contribute to the formation of such impurity levels and thus resulting in complexity of band structure. This causes CBM to extend toward Fermi level; resulting band gap energy is decreased. In this way, existence of these impurity states may help electrons to transit from valence band to conduction band. In the similar way, Ta insertion enhances the electrical conductivity of diamond and makes it an effective semiconductor. Similar trend is also reported by Zhang et al. [39]. Furthermore, incorporated-Ta in diamond acts like a donor, i.e., it donates electrons to diamond. Moreover, it can also be noticed that insertion of Ta in diamond causes its band structure to shift downwards as compared to that of pure diamond. Ta-incorporated diamond has a slightly deeper donor level, thus it creates ~2.0 eV of energy gap for majority spin (↑) and for minority spin (↓) ~1.9 eV of charge carriers as in [91]. Thus, decrease in band gap energy enhances the electrical conductivity of Ta-doped diamond films, and they act as a good semiconductor. The total densities of states for different percentages of Ta atoms doped in diamond lattice (1.56, 3.12 and 6.25% Ta) are presented in [91].

Due to the increasing percentage of Ta in diamond lattice, more levels are created in the conduction band, consequently, it meets the Fermi level and hence reduces the band gap. With the increasing content of Ta, some of such local impurity levels are also created in valence band. With the increase of Ta in the diamond lattice, band gap decreases; but, after an abrupt fall, the decrease is not very prominent as Ta starts reacting with carbon atoms forming TaC. Consequently, relative to that of pure diamond films, the energy gap of a substituted diamond abruptly falls to a very low value and thus of Ta-inserted diamond films.

10.3.4 Effects of Oxygen Incorporation into Diamond Films

The Band structures of diamond, which are incorporated with substitutional impurity of 1.56% oxygen, for majority and minority electron spins are presented in [91]. The formation of impurity states occur within the region of band gaps near conduction band minimum (CBM). In addition, Fermi level exists below CBM, therefore, inserted-oxygen in diamond behaves as a donor i.e., oxygen donates electrons to diamond. Furthermore, it can also be noticed that incorporation of oxygen in diamond causes its band structure to shift downwards as compared to that of pure diamond. Oxygen-substituted diamond has a slightly deeper donor level, thus it creates ~1.34 eV of energy gap for majority spin and ~1.10 eV for minority spin. BSs of oxygen-incorporated diamond with 3.12% of oxygen for spin-up and spin-down electrons are demonstrated and reported in [91], so that the impact of increasing oxygen concentration in diamond lattice can be seen. This causes the extension of CBM toward Fermi level; hence, band gap energy decreases further to ~0.46 eV in case of spin-up electrons and ~0.44 eV in case of spin-down electrons. Because of decrease in band gap energy, the electrical conductivity of oxygen-inserted diamond films enhances, thus making it a good semiconductor. Similar trend is reported by Zhang et al. [93]; anyhow, the various values of band gap energy can be associated with varied contents of oxygen insertion. Furthermore, the current DFT studies confirm that the insertion of oxygen into diamond structure enhances its electrical conductivity, thus oxygen-incorporated diamond films act as a semiconductor [94].

It is evident that the impurity states that occur in the region of band gap tend to extend CBM to Fermi level. It causes the band gap to decrease, and oxygen-incorporated diamond acts like a semiconductor. The partial density of states of diamond films doped with oxygen is presented in [91] and confirms the filling of both valence and conduction bands by 2p-O states. The appearance of the band at −55 eV confirms the shifting of CBM toward the Fermi level. By this behavior, the donor nature of oxygen has been approved. The present findings contradict the results of Long et al. [95] according to whom the oxygen plays the role of acceptor in diamond lattice through the creation of impurity states close to VBM. But our findings seem to be in good accord with the findings of Zhou et al. [93].

The isosurface charge density of the oxygen-doped diamond films is presented in [91]. For different regions, the charge density distribution is illustrated by different colors. The excess (positive) density of charge (blue) is observed across atoms that is seemed to be decreasing with the increasing distance from center as shown by the variation of colors from purple color to orange color (which describes negative charge density). The creation of single bond after the electrons sharing by two atoms is represented by blue color. It is clear that there is relatively greater charge between O and C atoms as compared to that of C and C atoms. This shows the stronger bonding of C–O as compared to C–C bonds. Between O and C atoms, the greater charge value exhibits that the oxygen defect combination can show as vacancy character (of defect states) related to bonds of C-atom. Same findings have been reported by Long et al. [95], however, in contradiction to that of Gali et al. [96], by whom the nature of chemical bonds between C–O is weaker due to the longer bond lengths of C–O relative to C–C bonds that cause in oxygen-incorporated diamond the lattice distortion.

10.4 Summary

In summary, it can be deduced that the electronic properties of Cu-doped 2D GaN calculated using DFT. The Cu dopants when Cu doped into 2D GaN monolayer, it become spin polarized; furthermore, this spin polarization calculation magnetizes p electrons of the three neighboring N atoms with help of p-d hybridization. The ferromagnetic coupling states are preferable among all Cu dopants rather than that of AFM coupling in Cu-doped 2D GaN. Hence, Cu is promising nonmagnetic dopant for 2D GaN monolayer to fabricate 2D-based DMSs, which are promising materials with reducing size and should be free from magnetic precipitates. The adsorption properties and the electronic interaction between Cu and deposited 2D ZnO atomically sheet have been performed using DFT. We predict that the Schottky contact is formed at the ZnO/Cu interface, and the charge accumulation has been observed at the interfacial layer of this hybrid system. There is a large amount of charge transfer between the 2D ZnO and Cu substrate. It is predicted that the electronic charges are accumulated at the interface as well as on the Zn and O atoms.

Band structure calculations lead to the semiconducting behavior of Ta-incorporated diamond films due to the creation of defects states inside the band gap region extending toward conduction band minimum. Resent DFT results support the behavior observed for the experimental electrical resistivity findings. Thus, tantalum incorporation in diamond films can be useful to fabricate n-type semiconducting diamond films for industrial applications. Electronic properties of oxygen-doped diamond have been studied using DFT calculations. It is observed that the highest occupied molecular orbital is localized at oxygen atom. In addition, C_4–O bond lengths are equivalent to those of C–C bonds of diamond indicating no lattice distortions in the oxygen-doped diamond. The substitution of oxygen into

diamond is thermodynamically favorable because of negative formation energy. Band structure calculations of oxygen-doped diamond demonstrate the creation of impurity states inside the band gap region which extend CBM toward Fermi level resulting in decrease of band gap energy, and hence, oxygen-doped diamond behaves as a semiconductor. The spin projected density of states calculations reveal significant contributions of O-2p states at the Fermi level with no appreciable magnetic moments appearing on oxygen or carbon atoms for all C_1–C_4 configurations leading to nonmagnetic semiconducting behavior of oxygen-doped diamond. Present DFT results verify that by adding oxygen into diamond lattice increases its conductivity and oxygen-doped diamond films behave like a semiconductor.

References

1. T. Dietl, H. Ohno, F. Matsukura, J. Cibert, D. Ferrand, Zener model description of ferromagnetism in zinc-blende magnetic semiconductors. Science **287**, 1019 (2000)
2. T. Dietl, A ten-year perspective on dilute magnetic semiconductors and oxides. Nat. Mater. **9**, 965 (2010)
3. I. Zutic, J. Fabian, S.D. Sarma, Spintronics: fundamentals and applications. Rev. Mod. Phys. **76**, 323 (2004)
4. S.D. Sarma, Ferromagnetic semiconductors: a giant appears in spintronics. Nat. Mater. **2**, 292 (2003)
5. I. Malajovich, J.J. Berry, N. Samarth, D.D. Awschalom, Persistent sourcing of coherent spins for multifunctional semiconductor spintronics. Nature **411**, 770 (2001)
6. H. Ohno, Making nonmagnetic semiconductors ferromagnetic. Science **281**, 951 (1998)
7. S.A. Wolf, D.D. Awschalom, R.A. Buhrman, J.M. Daughton, S.V. Molnar, M.L. Roukes, A. Y. Chtchelkanova, D.M. Treger, Spintronics: a spin-based electronics vision for the future. Science **294**, 1488 (2001)
8. J.S. Lee, J.D. Lim, Z.G. Khim, Y.D. Park, S.J. Pearton, S.N.G. Chu, Magnetic and structural properties of Co, Cr, V ion-implanted GaN. J. Appl. Phys. **93**, 4512 (2003)
9. J.R. Neal, A.J. Behan, R.M. Ibrahim, H.J. Blythe, M. Ziese, A.M. Fox, G.A. Gehring, Room-temperature magneto-optics of ferromagnetic transition-metal-doped ZnO thin films. Phys. Rev. Lett. **96**, 197208 (2006)
10. Y. Matsumoto, M. Murakami, T. Shono, T. Hasegawa, T. Fukumura, P. Ahmet, T. Chikyow, M. Kawasaki, S. Koshihara, H. Koinuma, Room-temperature ferromagnetism in transparent transition metal-doped titanium dioxide. Science **291**, 854 (2001)
11. M. Zaja, J. Gosk, E. Granka, M. Kaminska, A. Twardowski, B. Strojek, T. Szyszko, S. Podsiadlo, Possible origin of ferromagnetism in (Ga,Mn)N. J. Appl. Phys. **93**, 4715 (2003)
12. J.Y. Kim, J.H. Park, B.G. Park, H.J. Noh, S.J. Oh, J.S. Yang, D.H. Kim, S.D. Bu, W. Noh, H. J. Lin, H.H. Hsieh, C.T. Chen, Ferromagnetism induced by clustered co in co-doped anatase TiO_2 thin films. Phys. Rev. Lett. **90**, 017401 (2003)
13. K. Ando, H. Saito, Z. Jin, T. Fukumura, M. Kawasaki, Y. Matsumoto, H. Koinuma, Magneto-optical properties of ZnO-based diluted magnetic semiconductors. J. Appl. Phys. **89**, 7284 (2001)
14. S. Sonoda, S. Shimizu, T. Sasaki, Y. Yamamoto, H. Hori, Magnetic and transport characteristics on high Curie temperature ferromagnet of Mn-doped GaN. J. Appl. Phys. **91**, 7911 (2002)

15. D.B. Buchholz, R.P.H. Chang, J.H. Song, J.B. Ketterson, Room-temperature ferromagnetism in Cu-doped ZnO thin films. J. Appl. Phys. Lett. **87**, 082504 (2005)
16. M.S. Park, B.I. Min, Ferromagnetism in ZnO codoped with transition metals: Zn 1− x(FeCo)x O and Zn 1− x(FeCu)x O. Phys. Rev. B **68**, 224436 (2003)
17. C.H. Chien, S.H. Chiou, G.Y. Guo, Y.D. Yao, Electronic structure and magnetic moments of 3d transition metal-doped ZnO. J. Magn. Magn. Mater. **282**, 275 (2004)
18. X. Feng, Electronic structures and ferromagnetism of Cu-and Mn-doped ZnO. J. Phys.: Condens. Matter **16**, 4251 (2004)
19. L.H. Ye, A.J. Freeman, B. Delley, Half-metallic ferromagnetism in Cu-doped ZnO: density functional calculations. Phys. Rev. B **73**, 033203 (2006)
20. U. Grossner, S. Gabrielsen, T.M. Borseth, J. Grillenberger, A.Y. Kuznetsov, G. Svensson, Palladium Schottky barrier contacts to hydrothermally grown n-ZnO and shallow electron states. Appl. Phys. Lett. **85**, 2259 (2004)
21. H. Endo, M. Sugibuchi, K. Takahashi, S. Goto, S. Sugimura, K. Hane, Y. Kashi-waba, Schottky ultraviolet photodiode using a ZnO hydrothermally grown single crystal substrate. Appl. Phys. Lett. **90**, 121906 (2007)
22. C.L. Phillips, P.D. Bristowe, First principles study of the adhesion asymmetry of a metal/oxide interface. J. Mater. Sci. **43**, 3960 (2008)
23. K.S. Novoselov, A.K. Geim, S.V. Morozov, D. Jiang, Y. Zhang, S.V. Dubonos, V. Grigorieva, A.A. Firsov, Electric field effect in atomically thin carbon films. Science **306**, 666 (2004)
24. Y.B. Zhang, Y.W. Tan, H.L. Stormer, P. Kim, Experimental observation of the quantum Hall effect and Berry's phase in graphene. Nature **438**, 201 (2005)
25. K.S. Novoselov, A.K. Geim, S.V. Morozov, Two-dimensional atomic crystals. Proc. Natl. Acad. Sci. USA **102**, 10451 (2005)
26. Y.W. Son, M.L. Cohen, S.G. Louie, Half-metallic graphene nanoribbons. Nature **444**, 347 (2006)
27. E.J. Kan, Z.Y. Li, J.L. Yang, J.G.J. Hou, Half-metallicity in edge-modified zigzag graphene nanoribbons. Am. Chem. Soc. **130**, 4224 (2008)
28. O. Hod, V. Barone, J.E. Peralta, G.E. Scuseria, Enhanced half-metallicity in edge-oxidized zigzag graphene nanoribbons. Nano Lett. **7**, 2295 (2007)
29. W. Chen, Y.F. Li, G.T. Yu, C.Z. Li, S.B. Zhang, Z. Zhou, Z.F.J. Chen, Hydrogenation: a simple approach to realize semiconductor—half-metal—metal transition in boron nitride nanoribbons. Am. Chem. Soc. **132**, 1699 (2010)
30. M.S. Si et al., Intrinsic ferromagnetism in hexagonal boron nitride nanosheets. J. Chem. Phys. **140**, 204701 (2014)
31. Z.K. Tang, G.K.L. Wong, P. Yu, M. Kawasaki, A. Ohtomo, H. Koinuma, Y. Segawa, Room-temperature ultraviolet laser emission from self-assembled ZnO microcrystallite thin films. Appl. Phys. Lett. **72**, 3270 (1998)
32. O. Dulub, U. Diebold, G. Kresse, Novel stabilization mechanism on polar surfaces: ZnO (0001)-Zn. Phys. Rev. Lett. **90**, 016102 (2003)
33. C. Noguera, Polar oxide surfaces. J. Phys.: Condens. Matter **12**, 367 (2000)
34. A. Wander, F. Schedin, P. Steadman, A. Norris, R. McGrath, T.S. Turner, G. Thorn-ton, N.M. Harrison, Stability of polar oxide surfaces. Phys. Rev. Lett. **86**, 3811 (2001)
35. Y.K. Tseng, M.H. Chuang, Y.C. Chen, C.H. Wu, Synthesis of 1d, 2d, and 3d ZnO polycrystalline nanostructures using the sol-gel method. J. Nanotechnol. **8**, 712850 (2012)
36. M. Ullah, E. Ahmed, F. Hussain, A.M. Rana, R. Raza, Electronic structure calculations of oxygen-doped diamond using DFT technique. Microelectr. Eng. **146**, 26 (2015)
37. D. Lu, H.D. Li, S.H. Cheng, J.J. Yuan, X.Y. Lv, Fabrication and characteristics of nitrogen doped nanocrystalline diamond/p-type silicon heterojunction. Nano-Micro Lett. **2**, 56 (2010)
38. Y. Koide, M.Y. Liao, J. Alvarez, M. Imura, K. Sueishi, F. Yoshifusa, Schottky photodiode using submicron thick diamond epilayer for flame sensing. Nano-Micro Lett. **1**, 30 (2009)

39. Y. Zhang, L. Zhang, J. Zhao, L. Wang, G. Zhao, Y. Zhang, Doping of vanadium to nanocrystalline diamond films by hot filament chemical vapor deposition. Nanoscale Res. Lett. **7**, 441 (2012)
40. Z.J. Li, L. Wang, Y.J. Su, P. Liu, Y.F. Zhang, Semiconducting single-walled carbon nanotubes synthesized by S-doping. Nano-Micro Lett. **1**, 9 (2009)
41. S. Yamanaka, H. Watanabe, S. Masai, D. Takenuchi, H. Okushi, K. Kajimura, High-quality B-doped homoepitaxial diamond films using trimethylboron. Jpn. J. Appl. Phys. **37**, 1129 (1998)
42. A.T. Collins, The electronic and optical properties of diamond; do they favour device applications? Mater. Res. Soc. Symp. Proc. **162**, 3 (1990)
43. N. Fujimoro, T. Imai, H. Nakahata, H. Shiomi, Y. Nishibayashi, Epitaxial growth of diamond and diamond devices. Mater. Res. Soc. Symp. Proc. **162**, 23 (1990)
44. Y. Saito, Diamond synthesis from methane-hydrogen-water mixed gas using a microwave plasma. J. Mater. Sci. **23**, 842 (1988)
45. R. Kalish, Doping of diamond. Carbon **37**, 781 (1999)
46. S.A. Kajihara, A. Antonelli, J. Bernholc, R. Car, Nitrogen and potential n-type dopants in diamond. Phys. Rev. Lett. **66**, 2010 (1991)
47. S. Prawer, D.N. Jamieson, R.J. Walker, K.K. Lee, F. Watt, R. Kalish, Lattice substitution of phosphorous in diamond by MeV ion implantation and pulsed laser annealing. Diamond Films Technol. **6**, 351 (1997)
48. M.E. Zvanut, W.E. Carlos, J.A. Freitas Jr., K.D. Jamison, R.P. Hellmer, Identification of phosphorus in diamond thin films using electron paramagnetic resonance spectroscopy. Appl. Phys. Lett. **65**, 2287 (1994)
49. N. Arshi, J. Lu, C.G. Lee, B.H. Koo, F. Ahmed, Power-dependent structural, morphological and electrical properties of electron beam evaporated tantalum films. Electron. Mater. Lett. **9**, 841 (2013)
50. S. Talapatra, P.G. Ganesan, T. Kim, R. Vajtai, M. Huang, M. Shima, G. Ramanath, D. Srivastava, S.C. Deevi, P.M. Ajayan, Irradiation-induced magnetism in carbon nanostructures. Phys. Rev. Lett. **95**, 097201 (2005)
51. H. Ohldag, T. Tyliszczak, R. Hohne, D. Spemann, P. Esquinazi, M. Ungureanu, T. Butz, π-electron ferromagnetism in metal-free carbon probed by soft X-ray dichroism. Phys. Rev. Lett. **97**, 187204 (2007)
52. Y. Zhang, S. Talapatra, S. Kar, R. Vajtai, S.K. Nayak, P.M. Ajayan, First-principles study of defect-induced magnetism in carbon. Phys. Rev. Lett. **99**, 107201 (2007)
53. W.L. Wang, S. Meng, E. Kaxiras, Graphene nanoflakes with large spin. Nano Lett. **8**, 241 (2008)
54. Y.-W. Son, M.L. Cohen, S.G. Louie, Half-metallic graphene nanoribbons. Nature **444**, 347 (2006)
55. H. Ohno, Making nonmagnetic semiconductors ferromagnetic. Science **281**, 951 (1998)
56. S.A. Wolf, D.D. Awschalom, R.A. Buhrman, J.M. Daughton, S. von Molnár, M.L. Roukes, A.Y. Chtchelkanova, D.M. Treger, Spintronics: a spin-based electronics vision for the future. Science **294**, 1488 (2001)
57. S. Yamanaka, H. Watanabe, S. Masai, D. Takenuchi, H. Okushi, K. Kajimura, High-quality B-doped homoepitaxial diamond films using trimethylboron. Jpn. J. Appl. Phys. **37**, 1129 (1998)
58. S.B. Zhang, J.E. Northrup, Chemical potential dependence of defect formation energies in GaAs: application to Ga self-diffusion. Phys. Rev. Lett. **67**, 2339 (1991)
59. D.W. Boukhvalov, First principles modeling of the interactions of iron impurities with graphene and graphite. Phys. Status Solidi B **248**, 1347 (2011)
60. P.A. Brown, C. Xu, K.L. Shuford, Periodic trends of pnictogen substitution into a graphene monovacancy: a first-principles investigation. Chem. Mater. **26**, 5735 (2014)
61. D.W. Boukhvalov, M.I. Katsnelson, Destruction of graphene by metal adatoms. Appl. Phys. Lett. **95**, 023109 (2009)

62. G. Li, F. Li, X. Wang, M. Zhao, X. Liu, Gold atom and dimer adsorbed on perfect and defective graphene and boron nitride monolayer: A first-principles study. Physica E **59**, 235 (2014)
63. D. Xu, J. Zhao, X. Wang, A density functional theory study of the adsorption of bimetallic FenPtm clusters on defective graphene: structural, electronic and magnetic properties. J. Nanopart. Res. **15**, 1 (2013)
64. L.Y. Isseroff, E.A. Carter, Electronic structure of pure and doped cuprous oxide with copper vacancies: suppression of trap states. Chem. Mater. **25**, 253 (2013)
65. P. Blake, P.D. Brimicombe, R.R. Nair, T.J. Booth, D. Jiang, F. Schedin, L.A. Ponomarenko et al., Graphene-based liquid crystal device. Nano lett. **8**, 1704 (2008)
66. L. Feng, Simulation of crystal, electronic and magnetic structures, and gas adsorption of two dimensional materials, **20**, 5 (2014)
67. C.G. Van de Walle, J. Neugebauer, First-principles surface phase diagram for hydrogen on GaN surfaces. Phys. Rev. Lett. **88**, 066103 (2002)
68. Q.Z. Xue, Q.K. Xue, R.Z. Bakhtizin, Y. Hasegawa, I.S.T. Tsong, T. Sakurai, T. Ohno, Atomistic investigation of various GaN (0001) phases on the 6 H-SiC (0001) surface. Phys. Rev. B **59**, 12604 (1999)
69. A.R. Smith, R.M. Feenstra, D.W. Greve, M.S. Shin, M. Skowronski, J. Neugebauer, J.E. Northrup, GaN (0001) surface structures studied using scanning tunneling microscopy and first-principles total energy calculations. Surf. Sci. **423**, 70 (1999)
70. Q.K. Xue, Q.Z. Xue, R.Z. Bakhtizin, Y. Hasegawa, I.S.T. Tsong, T. Sakurai, T. Ohno, Structures of GaN (0001)-(2×2), -(4×4), and -(5×5) surface reconstructions. Phys. Rev. Lett. **82**, 3074 (1999)
71. A.R. Smith, R.M. Feenstra, D.W. Greve, J. Neugebauer, J.E. Northrup, Reconstructions of the GaN (000 1) surface. Phys. Rev. Lett. **79**, 3934 (1997)
72. T. Strasser, C. Solterbeck, F. Starrost, W. Schattke, Valence-band photoemission from the GaN (0001) surface. Phys. Rev. B **60**, 11577 (1999)
73. A.L. Rosa, J. Neugebauer, First-principles calculations of the structural and electronic properties of clean GaN (0001) surfaces. Phys. Rev. B **73**, 205346 (2006)
74. F.H. Wang, P. Krüger, J. Pollmann, Electronic structure of 1×1 GaN (0001) and GaN (0001) surfaces. Phys. Rev. B **64**, 035305 (2001)
75. R.G. Hernandez, W.L. Perez, M.G.M. Armenta, M.J.A. Rodríguez, Vanadium adsorption and incorporation at the GaN (0001) surface: a first-principles study. Phys. Rev. B **81**, 195407 (2010)
76. R.Q. Wu, G.W. Peng, L. Liu, Y.P. Feng, Ferromagnetism in Mg-doped AlN from ab initio study. Appl. Phys. Lett. **89**, 142501 (2006)
77. D.B. Buchholz, R.P.H. Chang, J.Y. Song, J.B. Ketterson, Room-temperature ferromagnetism in Cu-doped ZnO thin films. Appl. Phys. Lett. **87**, 082504 (2005)
78. F. Hussain, Y.Q. Cai, M.J.I. Khan, M. Imran, M. Rashid, H. Ullah, E. Ahmad, F. Kousar, S. A. Ahmad, Enhanced ferromagnetic properties of Cu doped two-dimensional GaN monolayer. Int. J. of Mod. Phys. **26**, 1 (2015)
79. Y. Ohno, D.K. Young, B. Beschoten, F. Matsukura, H. Ohno, D.D. Awschalom, Electrical spin injection in a ferromagnetic semiconductor heterostructure. Nature **402**, 790 (1999)
80. R. Fiederling, M. Keim, W. Reuscher, G. Ossau, A. Schmidt, A. Waag, L.W. Molenkamp, Injection and detection of a spin-polarized current in a light-emitting diode. Nature **402**, 787 (1999)
81. B. Sanyal, O. Bengone, S. Mirbit, Electronic structure and magnetism of Mn-doped GaN. Phys. Rev. B **68**, 205210 (2003)
82. S. Larentis, J.R. Tolsma, B. Fallahazad, D.C. Dillen, K. Kim, A.H. MacDonald, E. Tutuc, Band offset and negative compressibility in graphene-MoS_2 heterostructures. Nano Lett. **14**, 2039 (2014)
83. K.B. Sundaram, A. Khan, Work function determination of zinc oxide films. J. Vac. Sci. Technol. A **15**, 2 (1997)

84. Y.Q. Cai, A. Zhang, Y.P. Feng, C. Zhang, H.F. Teoh, G.W. Ho, Strain effects on work functions of pristine and potassium-decorated carbon nanotubes. J. Chem. Phys. **131**, 224701 (2009)
85. S. Ju, S. Kim, S. Mohammadi, D.B. Janes, Y.G. Ha, A. Facchetti, T.J. Marks, Interface studies of ZnO nanowire transistors using low-frequency noise and temperature-dependent I-V measurements. Appl. Phys. Lett. **92**, 022104 (2008)
86. V. Dose, W. Altmann, A. Goldmann, U. Kolac, J. Rogozik, Image-potential states observed by inverse photoemission. Phys. Rev. Lett. **52**, 1919 (1984)
87. A. Venugopal, L. Colombo, E.M. Vogel, Contact resistance in few and multilayer graphene devices. Appl. Phys. Lett. **96**, 013512 (2010)
88. C. Gong, G. Lee, B. Shan, E.M. Vogel, R.M. Wallace, K. Cho, First-principles study of metal graphene interfaces. J. Appl. Phys. **108**, 123711 (2010)
89. R. Tung, Formation of an electric dipole at metal-semiconductor interfaces. Phys. Rev. B. **64**, 20 (2001)
90. J. Bardeen, Surface states and rectification at a metal semi-conductor contact. Phys. Rev. **71**, 717 (1947)
91. M. Ullah, E. Ahmed, F. Hussain, A.M. Rana, R. Raza, H. Ullah, Electronic structure calculations of oxygen-doped diamond using DFT technique. Microelectron. Eng. **146**, 26 (2015)
92. C.X. Yan, Y. Dai, B.B. Huang, DFT study of halogen impurity in diamond. J. Phys. D Appl. Phys. **42**, 145407 (2009)
93. H. Zhou, Y. Yokoi, H. Tamura, S. Takami, M. Kubo, A. Miyamoto, Quantum chemical calculations of sulfur doping reactions in diamond CVD. Jpn. J. Appl. Phys. **40**, 2830 (2001)
94. M. Ullah, E. Ahmed, I.U. Hassan, M.J. Jackson, W. Ahmed, Controlling properties of micro crystalline diamond films using oxygen in a hot filament chemical vapor deposition system. J. Manuf. Technol. Res. **3**, 153 (2011)
95. R. Long, Y. Dai, L. Yu, Structural and electronic properties of oxygen-adsorbed diamond (100) surface. J. Phys. Chem. C **111**, 855 (2007)
96. A. Gali, J.E. Lowther, P. Deak, Defect states of substitutional oxygen in diamond. J. Phys.: Condens. Matter **13**, 11607 (2001)